# High water mobility on the ice-binding surface of a hyperactive antifreeze protein†

**Kristofer Modig,[a] Johan Qvist,[a] Christopher B. Marshall,‡[b] Peter L. Davies[b] and Bertil Halle*[a]**

***Received 11th February 2010, Accepted 17th May 2010***
**DOI: 10.1039/c002970j**

Antifreeze proteins (AFPs) prevent uncontrolled ice formation in organisms exposed to subzero temperatures by binding irreversibly to specific planes of nascent ice crystals. To understand the thermodynamic driving forces and kinetic mechanism of AFP activity, it is necessary to characterize the hydration behavior of these proteins in solution. With this aim, we have studied the hyperactive insect AFP from *Tenebrio molitor* (*Tm*AFP) with the $^{17}$O magnetic relaxation dispersion (MRD) method, which selectively monitors the rotational motion and exchange kinetics of water molecules on picosecond–microsecond time scales. The global hydration behavior of *Tm*AFP is found to be similar to non-antifreeze proteins, with no evidence of ice-like or long-ranged modifications of the solvent. However, two sets of structural water molecules, located within the core and on the ice-binding face in the crystal structure of *Tm*AFP, may have functional significance. We find that 2 of the 5 internal water molecules exchange with a residence time of $8 \pm 1$ μs at 300 K and a large activation energy of $\sim 50$ kJ mol$^{-1}$, reflecting intermittent large-scale conformational fluctuations in this exceptionally dense and rigid protein. Six water molecules arrayed with ice-like spacing in the central trough on the ice-binding face exchange with bulk water on a sub-nanosecond time scale. The combination of high order and fast exchange may allow these water molecules to contribute entropically to the ice-binding affinity without limiting the absorption rate.

## 1. Introduction

Antifreeze proteins (AFPs) contribute to freeze avoidance and tolerance in fish, insects and other organisms exposed to subzero temperatures.[1–5] Despite a remarkable structural diversity, all AFPs appear to bind to one or more faces of the ice crystal. According to the prevailing adsorption–inhibition mechanism, AFP binding arrests further growth of the ice crystal by imposing a convex shape on the ice–water interface between bound AFP molecules.[6–10] For this mechanism to be effective, several conditions must be satisfied. First, AFP binding must be essentially irreversible, otherwise ice would quickly accumulate during periods when the site is vacant. Second, the AFP molecule must provide a near-perfect match to the ice lattice to prevent water molecules from diffusing into the interface and becoming incorporated into the ice lattice. Third, the non-contacting surfaces of the AFP must have an unfavorable interaction with the ice surface to prevent the adsorbed AFP from being engulfed by the growing ice crystal. Fourth, since the thermal hysteresis activity of AFPs is a nonequilibrium phenomenon, the rate of AFP adsorption must be sufficiently high to arrest ice crystal growth.[11]

Atomic resolution structures of several AFPs have provided important clues about the determinants of ice binding.[3] The ice-binding surfaces of AFPs are relatively flat with polar groups that can engage in H-bonds with the ice surface, interspersed with nonpolar groups. Threonine side-chains, which combine these properties, are often abundant on the ice-binding surface of AFPs. While H-bonds undoubtedly play a role, the van der Waals (dispersion) attraction enabled by a high degree of shape complementarity between the AFP and the ice plane may be equally important.[3] Furthermore, entropic factors, which can only be gleaned indirectly from the protein structure, may also contribute substantially to the affinity and kinetics of ice binding. For example, the binding affinity may be enhanced by structural features, such as disulfide bonds, dense atomic packing and an extensive H-bond network, that rigidify the protein, thereby reducing the loss of configurational entropy upon binding.

Solvation effects are potentially important in any association process, but have so far received relatively little attention in connection with AFPs. The most prominent example is the classical hydrophobic effect, where release of ordered hydration water drives the association of two hydrophobic molecules or surfaces.[12–15] In the AFP context, hydration effects on association are more complex because only one of the surfaces is hydrophobic and the ice surface is atomically rough and dynamic.[16] A hydrophobic driving force

[a] *Department of Biophysical Chemistry, Center for Molecular Protein Science, Lund University, SE-22100 Lund, Sweden. E-mail: bertil.halle@bpc.lu.se*
[b] *Department of Biochemistry, Queen's University, Kingston, Ontario K7L 3N6, Canada. E-mail: peter.davies@queensu.ca*
† Electronic supplementary information (ESI) available: Further experimental details. See DOI: 10.1039/c002970j
‡ Present address: Division of Signaling Biology, Ontario Cancer Institute, University Health Network, Toronto, Ontario M5G 2M9, Canada.

for AFP binding to ice must be fine-tuned so as to avoid self-association or aggregation with other partly hydrophobic proteins.

While direct studies of AFP-ice interactions are experimentally challenging, valuable insights into the mechanism of ice-binding may also come from examining how AFPs interact with liquid water. The understanding of protein hydration has seen major advances in recent years,[17,18] including studies of deeply supercooled protein solutions,[19–21] but we are not aware of any experimental study of the hydration of an AFP. Here, we use $^{17}O$ magnetic relaxation dispersion (MRD), arguably the most direct probe of protein hydration dynamics,[22,23] to examine the hydration properties of an AFP in aqueous solution at temperatures from $+50$ °C to $-30$ °C, using femtoliter emulsion droplets to achieve the high degree of supercooling.[24]

We study the hydration of the hyperactive AFP (*Tm*AFP) from the yellow mealworm beetle, *Tenebrio molitor*.[25] The structure of *Tm*AFP has been determined by X-ray crystallography at 1.4 Å resolution[26] and by NMR; the crystal and solution structures are very similar.[27] *Tm*AFP has an exceptionally regular structure, built from 7 nearly identical 12-residue loops in a right-handed β-helix fold stabilized by 8 disulfide bonds and an extensive H-bond network, including a row of 5 internal water molecules (Fig. 1).[26] The repeating Thr-Cys-Thr motifs are arrayed to form a flat β-sheet with two ranks of Thr residues flanking a narrow trough occupied by a row of 6 water molecules H-bonded to the Thr hydroxyls on one side (Fig. 2). Mutation studies have identified this highly planar face of *Tm*AFP as the ice-binding surface, but it is not known whether these crystallographic water molecules are stably associated with the protein or if they are involved in ice binding.[28,29]

The $^{17}O$ MRD data presented here provide information about the internal water molecules as well as about the external hydration layer of *Tm*AFP. The internal water molecules are not directly involved in ice-binding, but their exchange kinetics reflect intermittent conformational fluctuations[30] that are of special interest to examine in view of the unusual rigidity of *Tm*AFP. In the external hydration layer, we were particularly interested in the exchange kinetics of the rank of

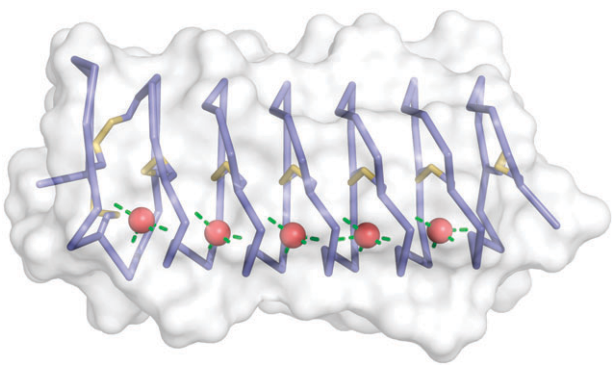

**Fig. 1** Crystal structure (1EZG[26] with added H atoms) of *Tm*AFP (isoform 2–14, N-terminus at left) showing the molecular surface (light grey), the backbone (blue) of the 7 β-helix loops reinforced by 8 disulfide bonds (yellow) and potential H-bonds (green dashed, $\leq$3.2 Å) with 5 internal water molecules (red).

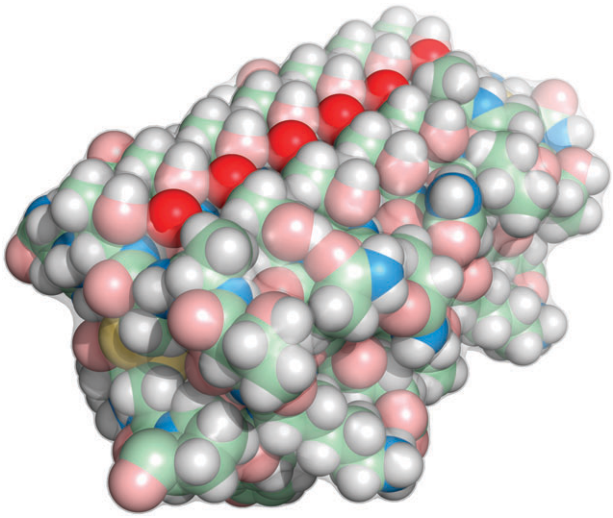

**Fig. 2** Crystal structure (1EZG[26] with added H atoms) of *Tm*AFP (isoform 2–14, C-terminus in front) showing the ice-binding face on top with ranks of 7 (left) and 4 (right) Thr side-chains and the sandwiched rank of 6 ordered water molecules (red).

6 water molecules on the ice-binding surface, which must play a role for both the affinity and the kinetics of ice binding. These water molecules have previously been examined by computational methods.[31] Furthermore, in view of the long-standing idea (still upheld by some researchers) that proteins and nucleic acids induce ice-like hydration structures of long-range,[32–34] it is clearly of interest to determine if this concept has any validity for AFPs, many of which contain arrays of residues that match the ice lattice. In this context, we compare our results on the global external hydration dynamics of *Tm*AFP with the results from a recent MD simulation study[35] of the hydration of a non-homologous but structurally similar AFP from another cold-tolerant insect, *Choristoneura fumiferana* (*Cf*AFP).

## 2. Materials and methods

### 2.1 Sample preparation

*Tenebrio molitor* (*Tm*) AFP isoform 4–9 was produced as a soluble recombinant protein in *E. coli* and purified by size-exclusion chromatography and reversed-phase HPLC.[28,36] The lyophilized protein was dissolved in a mixture of $D_2O$ (99.9% $^2H$, Cambridge Isotope Laboratories) and $^{17}O$-enriched $H_2O$ (19% $^{17}O$, Isotec/Sigma-Aldrich) with deuteron fraction, $X_D = 0.476$. A low pH* of 2.4 (where the protein has a net charge of $+6$) was used to minimize protein self-association. (Here, pH* denotes the pH meter reading uncorrected for the H/D isotope effect.) The solution was split in two identical samples, A and B, which also contained 0.02% sodium azide, but no buffer. Isoform 4–9 studied here is very similar to isoform 2–14 used for structure determination.[26,27] Both have 84 residues and all residues on the ice-binding face are the same.[25] Of the 5 residues that differ between the isoforms, 4 are on the right-hand flank of the ice-binding surface as depicted in Fig. 2.

Sample A was used for $^2$H and $^{17}$O relaxation measurements over a period of several months following sample preparation. Sample B was stored at 4 °C for 6 years and was then used for low-temperature $^{17}$O relaxation measurements. Complete amino-acid analyses, performed on the two samples 6 years apart, confirmed the amino-acid composition of the 4–9 isoform[25] and did not indicate any significant changes in composition during storage of sample B (Table S1†). The protein concentration obtained from the amino-acid analyses was 2.17 mM for sample A and 2.16 mM for sample B (after storage). However, pH* of sample B had increased from 2.4 to 3.1, which could be accounted for by acid hydrolysis (deamidation) of 2 of the 10 Asn or Gln residues in each molecule of *Tm*AFP isoform 4–9.

Two further controls of the integrity of sample B were performed. First, a HMQC NMR spectrum recorded from sample B (at natural $^{15}$N abundance) was well dispersed and did not indicate any significant structural modification (Fig. S1†). Second, water $^2$H longitudinal relaxation measurements performed on sample B at 27 °C and three magnetic fields (4.6–12 MHz) coincided within experimental accuracy (<1%) with the earlier results for sample A (Table S2†). The solvent deuteron fraction, $X_D$, of sample B, determined by mass spectrometry (Iso-Analytical Ltd, Cheshire, UK), was 0.369 ± 0.005. The reduction of the deuteron fraction as compared to sample A is attributed to water exchange with the atmosphere through the cap of the NMR tube.

Relaxation measurements at temperatures below the equilibrium freezing point of the solvent were performed on an emulsion sample, prepared[20,21] by mixing *Tm*AFP sample B with an equal volume of *n*-heptane (>99%, HPLC grade, Sigma) containing 3% (w/w) of the nonionic emulsifier sorbitan tristearate (Sigma). As a control of possible perturbations introduced by the droplet interface, the $^{17}$O relaxation rate, $R_1$, was measured at 81 MHz and 27 °C on the *Tm*AFP solution and on the pure-solvent reference before and after emulsification. The two $R_1$ values differed by 0.2% for both samples, which is within the experimental accuracy (Table S3†). The same emulsification protocol has been used for several other proteins without detectable perturbation.[20,21] Indeed, in a typical emulsion droplet of 10 μm diameter, only 0.3% of the protein molecules are located within 50 Å of the interface.

### 2.2 Spin relaxation measurements

The relaxation rate, $R_1$, of the water $^{17}$O longitudinal magnetization was measured with ~0.5% accuracy.[20,21] For sample A, $R_1$ was recorded as a function of resonance frequency (2.2–81 MHz) at 3 temperatures (27, 40 or 50 °C). For sample B, $R_1$ was recorded as a function of temperature (from +27.0 to −30.7 °C) at a fixed $^{17}$O resonance frequency (81.3 MHz on a Varian Unity Plus 600 spectrometer). The results of these two types of measurement series are referred to as a magnetic relaxation dispersion (MRD) profile (sample A) and a temperature profile (sample B), respectively. For the MRD profile, we used Varian Unity Plus 500 and 600 and Bruker Avance DMX 200 and 100 spectrometers and, at lower frequencies, a field-variable iron-core magnet (Drusch EAR-35N) interfaced to a Tecmag console. A limited MRD data set obtained at 70 °C indicated partial unfolding and a subsequent room-temperature HSQC NMR spectrum showed that this unfolding was irreversible. The analysis was therefore restricted to $R_1$ data obtained at temperatures ≤50 °C.

Water $^2$H MRD profiles were also acquired at each temperature. These data are fully consistent with the expected rotational correlation time of *Tm*AFP (section 2.4). The excess (above pure solvent) $^2$H $R_1$ is dominated by labile deuterons in side-chain COOD and OD groups in fast (COOD) or intermediate (OD) exchange with water deuterons. For this reason, the $^2$H MRD data do not provide clear-cut information about hydration dynamics and will not be discussed further.

At each point of the temperature profile, the $^{17}$O relaxation rates for the *Tm*AFP sample and for a pure-solvent reference sample were measured repeatedly (typically, every 2 min) until stable results were obtained. The reported $R_1$ is an average of the last 4–6 measurements. At least 20 min (30–40 min below −25 °C) was allowed for temperature equilibration. The temperature was checked before and after each set of $R_1$ measurements by inserting a copper-constantan thermocouple immersed in an ethanol–water mixture in the probe. Because the $^{17}$O resonance from ice is broadened beyond detection, any freezing of water is observed as a reduction of the $^{17}$O peak intensity. At −30.7 °C about half of the emulsion droplets in the *Tm*AFP sample had frozen after one hour, resulting in a larger standard deviation of the individual $R_1$ measurements (0.7%) at this temperature. At lower temperatures (−31.2 °C and below), the *Tm*AFP sample (but not the reference sample) froze too quickly to allow accurate $R_1$ measurements.

### 2.3 Analysis of relaxation data

The water $^{17}$O relaxation rate, $R_1$, in a protein solution exceeds the bulk-water value, $R_1^0$, because the water molecules that interact with the protein rotate more slowly than in bulk water. NMR relaxation studies of model systems[37,38] as well as MD simulations[35,39,40] have shown that the dynamical perturbation of water rotation induced by the protein is short-ranged. (Note that many MD studies use a uniform radial cutoff to delimit the first hydration layer of the protein, which then usually does not include the first hydration shell of apolar groups.) To a good approximation, the perturbation can thus be attributed to the $N_H$ water molecules that interact directly with the external protein surface, the first hydration layer, and to the $N_I$ internal water molecules that are buried within the protein structure. For *Tm*AFP, $N_H$ = 366 is obtained by dividing the solvent-accessible surface area of *Tm*AFP (probe radius 1.7 Å) by the average surface area, 10.75 Å$^2$, occupied by one water molecule at the surface.[41] Furthermore, $N_I$ = 5 is obtained from the crystal structure[26] of *Tm*AFP (Fig. 1). From the known protein concentration in our samples, we calculate the water/protein mole ratio, $N_W$ = 25 300, with an accuracy of 1–2%.

In general, the measured $^{17}$O spin relaxation rate has contributions from all three water classes: bulk water, (external) hydration water and internal water. The relative importance of each class depends on the residence time and rotational correlation time of the water molecules. In the fast-exchange limit, when the mean residence time (the inverse of

the exchange rate) is much shorter than the intrinsic $^{17}O$ spin relaxation rate (a few ms for hydration water, a few μs for internal water), the observed relaxation rate is simply a population-weighted average of the intrinsic rates. This limit invariably applies to hydration water, but not necessarily to internal water. In the so-called extreme-narrowing limit, when the rotational correlation time is short compared to the inverse of the highest resonance frequency, $(2\pi \times 600\ \mathrm{MHz})^{-1} \approx 0.3$ ns, the corresponding spin relaxation rate is constant in the examined frequency window. This limit applies to the vast majority of water molecules in the hydration layer, but not to internal water molecules or hydration waters residing in deep surface pockets.[20]

Under rather general conditions, the observed relaxation rate can thus be written as[22,23]

$$R_1(\omega_0,T)=\left(1-\frac{N_\mathrm{H}+N_\mathrm{I}}{N_\mathrm{W}}\right)R_1^0(T)+\frac{1}{N_\mathrm{W}}\sum_{k=1}^{N_\mathrm{H}}R_{1,k}^\mathrm{H}(\omega_0,T)+\frac{1}{N_\mathrm{W}}\sum_{k=1}^{N_\mathrm{I}}[\tau_k^\mathrm{I}(T)+1/R_{1,k}^\mathrm{I}(\omega_0,T)]^{-1} \quad (1)$$

where $\tau_k^\mathrm{I}$ is the mean residence time of internal water molecule $k$ and $\omega_0$ is the (angular) resonance frequency. The intrinsic relaxation rates (X = H or I) are given by[22,23]

$$R_{1,k}^\mathrm{X}(\omega_0,T)=\omega_\mathrm{Q}^2[0.2J_k^\mathrm{X}(\omega_0,T)+0.8J_k^\mathrm{X}(2\omega_0,T)] \quad (2)$$

where $\omega_\mathrm{Q} = 7.6 \times 10^6\ \mathrm{s}^{-1}$ is the $^{17}O$ nuclear quadrupole frequency. The spectral density function is taken to be of the Lorentzian form,

$$J_k^\mathrm{X}(\omega,T)=\frac{S_k^2\tau_{\mathrm{C},k}^\mathrm{X}(T)}{1+[\omega\tau_{\mathrm{C},k}^\mathrm{X}(T)]^2} \quad (3)$$

where $S_k$ is an orientational order parameter.[23] Finally, the effective rotational correlation time is given by[20,23]

$$\tau_{\mathrm{C},k}^\mathrm{X}(T)=\left[\frac{1}{\tau_\mathrm{P}(T)}+\frac{1}{\tau_k^\mathrm{X}(T)}\right]^{-1} \quad (4)$$

where $\tau_\mathrm{P}(T)$ is the rotational correlation time of the protein and $\tau_k^\mathrm{X}(T)$ is either the rotational correlation time (X = H) or the residence time (X = I) of water molecule $k$.

Depending on the exchange rates, only some of the $N_\mathrm{I}$ crystallographically identified internal water molecules may contribute to $R_1$ at a given temperature. If the $N_\mathrm{I}' \leq N_\mathrm{I}$ contributing internal water molecules have the same residence time, $\tau_\mathrm{I}$, and if $N_\mathrm{I}' \ll N_\mathrm{W}$ and $\tau_\mathrm{I} \gg \tau_\mathrm{P}$, then we can combine eqn (1)–(4) to obtain (after a minor approximation[22,23])

$$R_1(\omega_0,T)=\left\{1+\frac{N_\mathrm{H}}{N_\mathrm{W}}[\xi(\omega_0,T)-1]\right\}R_1^0(T)+\frac{\hat{N}_\mathrm{I}'(T)}{N_\mathrm{W}}\omega_\mathrm{Q}^2S_\mathrm{I}^2\left\{\frac{0.2\hat{\tau}_\mathrm{P}(T)}{1+[\omega_0\hat{\tau}_\mathrm{P}(T)]^2}+\frac{0.8\hat{\tau}_\mathrm{P}(T)}{1+[2\omega_0\hat{\tau}_\mathrm{P}(T)]^2}\right\} \quad (5)$$

with the renormalized occupation number, $\hat{N}_\mathrm{I}'$, and correlation time, $\hat{\tau}_\mathrm{P}$, given by

$$\frac{\hat{N}_\mathrm{I}'(T)}{N_\mathrm{I}'}=\frac{\hat{\tau}_\mathrm{P}(T)}{\tau_\mathrm{P}(T)}=[1+\omega_\mathrm{Q}^2S_\mathrm{I}^2\tau_\mathrm{P}(T)\tau_\mathrm{I}(T)]^{-1/2} \quad (6)$$

In eqn (5), we have also introduced the apparent dynamic perturbation factor (ADPF), $\xi(\omega_0, T)$, defined as[20]

$$\xi(\omega_0,T)\equiv\frac{\langle R_1^\mathrm{H}(\omega_0,T)\rangle}{R_1^0(T)}\leq\frac{\langle\tau_\mathrm{H}(T)\rangle}{\tau_0(T)}\equiv\xi(T) \quad (7)$$

The frequency-dependent ADPF, $\xi(\omega_0, T)$, is a lower bound on the true DPF, $\xi(T)$, which is a measure of the relative slowing down of water rotation in the external hydration layer.[20] In other words, the DPF is the ratio of the mean rotational correlation time for hydration water, $\langle\tau_\mathrm{H}\rangle$, and the bulk-water rotational correlation time, $\tau_0$, at the same temperature. To obtain the DPF from the ADPF, the distribution of correlation times in the hydration layer must be known.[20]

The three MRD profiles at 27, 40 and 50 °C were fitted globally with eqn (5)–(7) under the assumption of frequency-independent ADPF. The temperature dependence of the residence time was described by the Arrhenius law: $\tau_\mathrm{I}(T) = \tau_\mathrm{I}(T_0)\exp[(E_\mathrm{I}/R)(1/T - 1/T_0)]$. The protein rotational correlation time, $\tau_\mathrm{P}(T)$, was taken from hydrodynamic calculations (section 2.4) and the known solvent viscosity. The ADPF, $\xi(T)$, was taken from the high-frequency temperature profile (see below) at $T_0$ and was treated as a single adjustable parameter at the two higher temperatures. The additional three adjustable parameters in the joint fit were $\hat{N}_\mathrm{I}'S_\mathrm{I}^2$, $\tau_\mathrm{I}(T_0)S_\mathrm{I}^2$ and $E_\mathrm{I}$. All other quantities in eqn (5)–(7) are known.

The high-frequency temperature profile was analyzed with the first term of eqn (5), after correction for the small internal-water contribution (the second term) at the highest temperatures. The temperature dependence of the ADPF, $\xi(\omega_0, T)$, was modeled by assuming a power-law distribution for the rotational correlation time of the $N_\mathrm{H}$ water molecules in the hydration layer: $f(\tau) \propto \tau^{-\nu}$.[20] This model contains as adjustable parameters the power-law exponent, $\nu$, and the activation energy, $E_\mathrm{H}^-$, for water rotation at the lower boundary of the distribution.[20] All fits were performed with the Marquardt–Levenberg nonlinear least-squares algorithm.

### 2.4 Hydrodynamic calculations

The isotropic rank-2 rotational correlation time, $\tau_\mathrm{P}$, for *Tm*AFP was obtained from molecular hydrodynamics calculations using the program[42] HydroPro v. 7c with the recommended[43] effective hydrodynamic radius of 3.0 Å and one of two symmetry-related *Tm*AFP monomers from the 1.4 Å crystal structure 1EZG.[26] (The crystal structure lacks two C-terminal residues and it refers to isoform 2–14, which differs in five residues from the isoform 4–9 examined here.[25] These differences are deemed insignificant for the $\tau_\mathrm{P}$ calculation.) Extrapolation from 8 calculations with the minibead radius in the range 0.8–2.0 Å yielded $\tau_\mathrm{P} = 4.39$ ns for 20 °C and a nominal solvent viscosity $\eta_0 = 1.00$ cP. To obtain $\tau_\mathrm{P}$ at the experimental temperatures and $H_2O/D_2O$ solvent viscosities, we used the scaling $\tau_\mathrm{P} \propto \eta_0/T$. The result calculated here from

 

the crystal structure is in excellent agreement with the $\tau_R$ values deduced from $^{15}N$ relaxation data.[27] Because of its elongated shape, *Tm*AFP undergoes anisotropic rotational diffusion. However, for the computed anisotropy, $D_{R,\parallel}/D_{R,\perp} = 1.6$, the resulting deviation from Lorentzian spectral density function is not likely to be apparent in our MRD data.

## 3. Results

### 3.1 MRD profiles

The water $^{17}O$ MRD profiles acquired at 27, 40 and 50 °C (Fig. 3) exhibit a dispersion (frequency dependence), which unambiguously demonstrates that some water molecules interacting with *Tm*AFP have residence times longer than a few nanoseconds at these temperatures. While the locations of the long-lived water molecules cannot be established from the MRD data, the available structural information[26] leaves only two possibilities: (i) the 5 internal water molecules (Fig. 1), or (ii) the 6 ordered water molecules on the ice-binding surface (Fig. 2).

From previous MRD studies of more than two dozen proteins with known structures,[17,18,23,44] it is clear that these two groups of water molecules must have widely different residence times. An external (partly solvent-exposed) water molecule can have a residence time in the nanosecond range (at ambient temperature) only if it occupies a deep pocket where strong H-bonds with the protein must be broken before another water molecule can take its place. Each of the 6 ordered external water molecules on the ice-binding face of *Tm*AFP makes one strong H-bond (2.7–2.8 Å) with a Thr hydroxyl group from the longer rank of 7 Thr residues (Fig. 2). Weaker polar interactions are possible with the Thr carbonyl oxygen and the nearby Cys peptide nitrogen, but these two atoms are strongly (2.9 Å) H-bonded to each other. Since the Thr side-chain is fully solvent-exposed, each of the 6 ordered water molecules could probably exchange with bulk water in a concerted manner without temporarily sacrificing any strong H-bond. The residence time for these water molecules is therefore unlikely to exceed 1 ns at 27 °C. A fit to the 50 °C data shows that the correlation time is very close to the expected protein rotational correlation time at this temperature, $\tau_P = 2.4$ ns (section 2.4). According to eqn (4), if the 6 ordered external waters are responsible for the observed $^{17}O$ dispersion, they must thus have a residence time considerably longer than 2.4 ns at 50 °C. This is highly unlikely. Furthermore, the small dispersion amplitude would then correspond to a small orientational order parameter ($S^2 \approx 0.2$–$0.3$) for these water molecules, even though they have a high degree of positional order (the thermal *B*-factors for these water molecules are as low as for the protein atoms of the exceptionally rigid protein).[26] These considerations suggest that the observed $^{17}O$ dispersion is produced, not by external hydration waters, but by (some of) the 5 internal water molecules in *Tm*AFP (Fig. 1).

Since the internal water molecules are completely enclosed within an exceptionally rigid protein matrix, we expect them to have residence times in the microsecond range or longer.

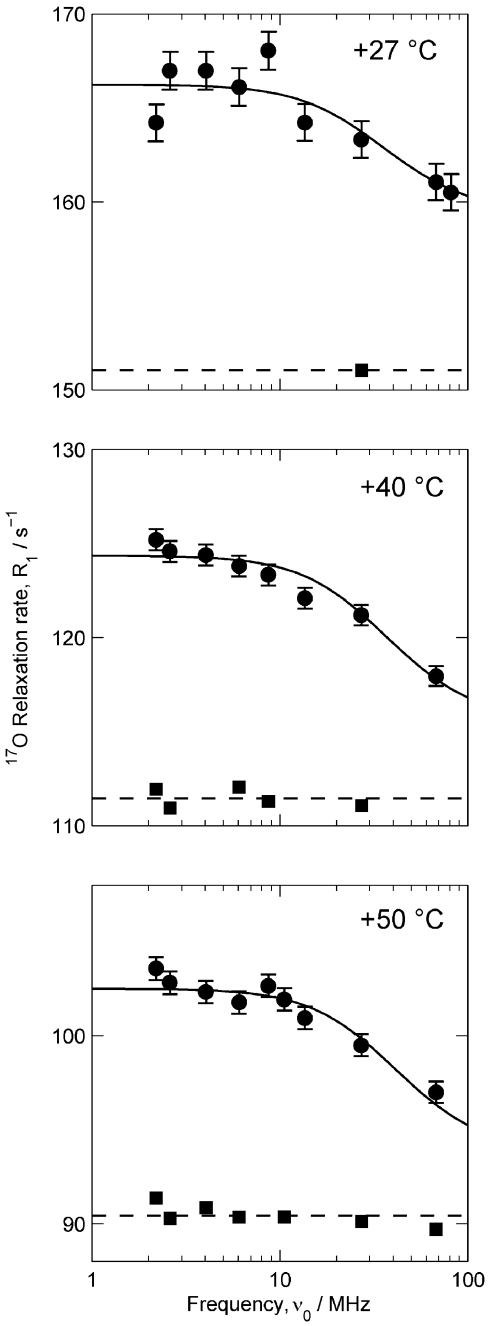


**Fig. 3** Water $^{17}O$ MRD profiles from a 2.17 mM solution of *Tm*AFP (circles) and from a pure-solvent reference sample (squares) at 27, 40 and 50 °C. The solid curves resulted from a global fit to all data (see text).

In fact, they might all be in the slow-exchange limit and therefore not contribute to the $^{17}O$ dispersion. If they contribute, an intermediate-exchange situation is likely. According to eqn (1), the internal waters should then contribute more to the dispersion at higher temperatures where the exchange is faster. This behavior is indeed observed (Fig. 3), implying that the residence time is in the microsecond range (comparable to the intrinsic $^{17}O$ relaxation time). This observation definitely rules out the 6 external hydration waters as the origin of the $^{17}O$ dispersion.

For the quantitative analysis, we jointly fitted the three MRD profiles in Fig. 3 using eqn (5)–(7) as described in section 2.3. The parameter values deduced from the fit ($\chi^2 = 1.3$) are $N'_I S_I^2 = 1.9 \pm 0.2$, $\tau_I(27\ ^\circ C) S_I^2 = 7.0 \pm 1.3$ μs, $E_I = 53 \pm 14$ kJ mol$^{-1}$ and $\xi(40–50\ ^\circ C) = 3.6 \pm 0.3$. Given the exceptionally high packing density[26] and rigidity[27] and the extensive internal H-bond network (including the internal waters; see Fig. 1), we expect[45,46] that the internal water molecules have very little orientational freedom and, consequently, that the order parameter, $S_I$, approaches its maximum value of 1. Adopting $S_I^2 = 0.9$, the fit results imply that $N'_I = 2.1 \pm 0.2$ internal water molecules have a mean residence time $\tau_I = 8 \pm 1$ μs at 27 °C, while the remaining 3 internal water molecules seen in the *Tm*AFP structure (Fig. 1) exchange too slowly ($\tau_I \gg 10$ μs) to make a significant contribution to the $^{17}$O spin relaxation rate.

### 3.2 Temperature profile

To study the dynamics of the external hydration layer over a wide temperature range extending into the supercooled regime, we contained the *Tm*AFP solution in femtoliter water/heptane emulsion droplets.[24] With a typical diameter of 10 μm, the aqueous emulsion droplets are sufficiently small that only a negligible fraction of the combined aqueous phase freezes by heterogeneous nucleation (at temperatures not far below the equilibrium freezing point of the solution), yet sufficiently large that only a negligible fraction of the protein solution in each droplet may be influenced by the water–oil interface (saturated with protein-repelling sorbitan head-groups). In this way, relaxation measurements on the supercooled aqueous protein solution could be performed down to −30 °C. To minimize the contribution from internal water molecules, the $^{17}$O relaxation rate, $R_1$, was measured at a high frequency (81 MHz). At this frequency, the internal-water contribution to the excess relaxation rate, $R_1 - R_1^0$, is <10% at the highest temperatures and negligible at subzero temperatures.

In Fig. 4 we have plotted the quantity $1 + (N_W/N_H)(R_1/R_1^0 - 1)$ obtained from the experimental results $R_1$, $R_1^0$ and $N_W$ and from the structure-based number, $N_H$, of water molecules in the first hydration layer (section 2.3). According to eqn (5), this quantity equals the apparent dynamic perturbation factor (ADPF), $\xi(\omega_0, T)$, if the internal-water contribution can be neglected. For the quantitative analysis of the temperature profile, we first subtracted the small internal-water contribution as given by the second term in eqn (5), using the parameter values derived from the MRD profiles (section 3.1). We then modeled the temperature dependence of the mean relaxation rate $\langle R_1^H(\omega_0, T)\rangle$ by assuming a power-law distribution of rotational correlation times in the hydration layer.[20] The two-parameter fit (Fig. 4) yields $\nu = 2.08 \pm 0.02$ for the power-law exponent and $E_H^- = 31 \pm 1$ kJ mol$^{-1}$ for the activation energy. As seen previously for three other proteins without antifreeze activity,[20] the ADPF exhibits a broad maximum just below 0 °C and falls off markedly at lower temperatures (Fig. 4).

Having determined the model parameters, we can compute the true DPF, $\xi(T)$, as defined in eqn (7).[20] In Fig. 5, we compare the DPF curve for *Tm*AFP with two non-antifreeze proteins: mammalian ubiquitin (mUb, 8.6 kDa, pH 5.0) and bovine β-lactoglobulin (BLG, 18.4 kDa, pH 2.7).[20] For all three proteins, the DPF curve has a broad maximum between −10 and −15 °C, where the DPF is 4.9 (mUb), 7.4 (BLG) and 9.6 (*Tm*AFP). The maximum in the DPF curves occurs at the temperature where the (mean) activation energy for water rotation in the hydration layer is the same as in bulk water.[20]

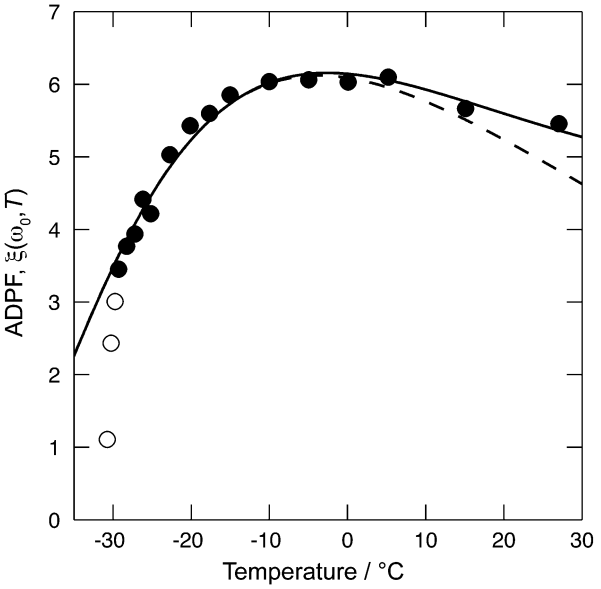


**Fig. 4** Temperature dependence of the $^{17}$O ADPF measured at 81 MHz on emulsified samples of 2.16 mM *Tm*AFP solution and pure solvent. The curve resulted from a two-parameter fit (see text) to the solid data points. The difference between the solid and dashed curves is the contribution from internal water molecules.

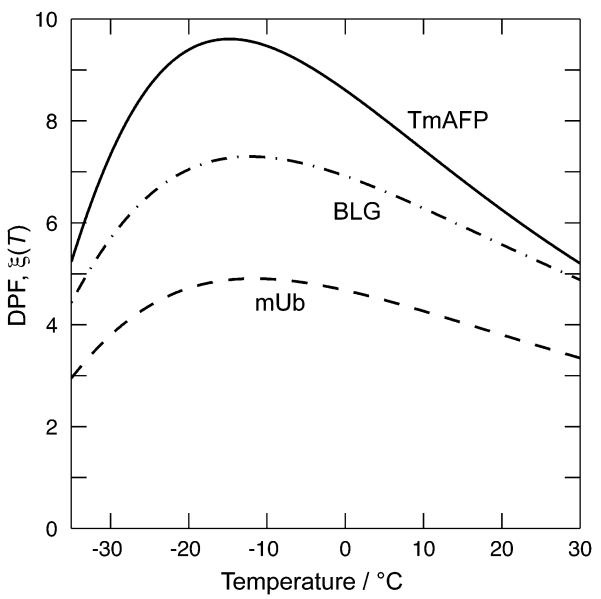


**Fig. 5** Temperature dependence of the true $^{17}$O DPF for *Tm*AFP and two previously studied[20] proteins: β-lactoglobulin (BLG) and ubiquitin (mUb).

 

At lower temperatures, hydration water thus rotates with smaller activation energy than bulk water.

The homogeneous nucleation temperature, $T_H$, defined as the practical limit of supercooling of the aqueous emulsion droplets on the present experimental time scale (tens of minutes), is about −35.5 °C for the mixed $H_2O/D_2O$ solvent used here. For the *Tm*AFP solution, we estimate $T_H = -30.5$ °C (see section 2.2). This 5 °C increase of $T_H$ observed for *Tm*AFP is larger than that seen previously for non-antifreeze proteins studied in $H_2O$ (<2 °C upshift).[20] We cannot exclude the possibility that the larger effect on $T_H$ of *Tm*AFP is related to its affinity for the ice surface. At these very low temperatures, *Tm*AFP might simultaneously nucleate and inhibit ice growth. A significant fraction of the protein could then be bound to very small ice crystals, thereby reducing the solvent-accessible protein surface area and reducing the effective ADPF, as seen at the lowest temperatures in Fig. 4. For this reason, the data points at the three lowest temperatures (≤−29.7 °C, open symbols) were excluded from the power-law fit. In any case, inclusion of these data points has a negligible effect on the fit and parameter values ($\nu = 2.07 \pm 0.02$, $E_H^{\ddagger} = 30 \pm 1$ kJ mol$^{-1}$).

## 4. Discussion

### 4.1 Internal water molecules

The 5 internal water molecules in *Tm*AFP play a structural role but are not directly involved in ice binding. Indeed, the hyperactive *Cf*AFP from *Choristoneura fumiferana* (spruce budworm) has a similar β-helical structure but lacks internal water molecules.[47] Nevertheless, the internal waters in *Tm*AFP may contribute indirectly to its antifreeze activity by helping to maintain a rigid structure that provides for efficient recognition and strong binding to ice. In particular, the internal H-bond network enabled by the internal water molecules in *Tm*AFP may enhance the ice-binding affinity by further reducing the binding-induced loss of configurational entropy.

Compared to most other globular proteins, *Tm*AFP stands out for its high packing density and rigidity, with 8 disulfide bonds and uniformly high backbone order parameters.[27] On the basis of the molecular volume computed from the crystal structure,[26] with allowance for the two missing residues, the partial specific volume of *Tm*AFP is 0.62 cm$^3$ g$^{-1}$, compared to the typical value of 0.73 cm$^3$ g$^{-1}$. The 5 internal water molecules, tightly embedded in this rigid framework and connected to it by a full complement of H-bonds, clearly constitute an integral part of the protein. Nevertheless, the present $^{17}$O MRD data show that 2 of them exchange with external water molecules on a 10 μs time scale at 27 °C (130 μs at 0 °C). This finding implies that *Tm*AFP undergoes intermittent structural fluctuations on this time scale. Presumably, we are observing the water molecules at the less rigid ends[27] of the β-helix. Residence times for internal water molecules in other proteins range from tens of nanoseconds to hundreds of microseconds (at room temperature).[30,45] Whereas the three central water molecules may be more long-lived, the two peripheral water molecules conform to this general picture.

### 4.2 External hydration layer

If the physical properties of the external hydration layer are critical for the antifreeze activity of *Tm*AFP, these properties should deviate from the generic hydration behavior of proteins without antifreeze activity. Since AFPs have evolved to bind with high affinity to the growing planes of hexagonal ice crystals, their interaction with water molecules in the liquid state may also be peculiar. Specifically, the ice-binding AFP surface might impose an ice-like structure in the adjacent hydration layer. The surface-induced perturbation of the solvent could then extend further for AFPs than for other proteins, where already the second water layer is virtually indistinguishable from bulk water. An extended ice-like hydration layer might promote the early recognition of the ice surface and facilitate fusion of the protein with the ice lattice.[35]

Before AFPs had been discovered, it was proposed that biological macromolecules, by providing a matching complement of interaction sites, induce an ice-like structure in the surrounding water that may extend several hundred Å from the surface.[32–34] Similar views are still promoted by some researchers, even though more recent experiments and simulations have demonstrated that the perturbation is essentially limited to the first water layer and that the magnitude of this perturbation is modest, with less than two-fold slowing down of rotational motions for the majority of the first-layer water molecules.[18–20] Nevertheless, it might be argued that the ice-like hydration concept is relevant for AFPs, which do have surfaces that match the ice lattice in terms of shape complementarity and H-bonding partners. Perhaps the most significant result of the present study is to demonstrate that the dynamic properties of the hydration layer of this hyperactive AFP are *not* ice-like. As seen from Fig. 5, the hydration dynamics of *Tm*AFP are not qualitatively different from that of proteins without ice-matching surfaces. And, as argued in the following paragraphs, the quantitative differences can be rationalized without invoking unusual hydration behavior for *Tm*AFP.

The dynamic perturbation factor (DPF), which is a measure of the slowing down of water rotation in the hydration layer relative to bulk water, is 6.3 for *Tm*AFP at 20 °C, similar to β-lactoglobulin (5.7) but significantly larger than for ubiquitin (3.8). To understand this variation, it must be recognized that the small number of water molecules in the long-correlation-time tail of the power-law distribution make a disproportionately large contribution to the arithmetic average expressed by the DPF. Thus, if we disregard the slowest 10% of the hydration layer, the DPF profiles for the remaining 90% differ very little among different proteins,[20] including *Tm*AFP. The larger DPF for β-lactoglobulin as compared to ubiquitin can be explained by a larger number of secluded hydration sites, deep surface pockets where a water molecule experiences strong orientational constraints for extended periods of time (up to ~1 ns at room temperature). These special hydration sites are evident in the crystal structure of β-lactoglobulin and they are manifested in MRD profiles at lower temperatures, where the correlation times of these water molecules are sufficiently long (>1 ns) to give rise to a frequency dependence.[20]

From the high-resolution crystal structure of *Tm*AFP,[26] it is clear that the larger DPF for this protein can be attributed to the rank of 6 water molecules in the narrow trough between the two Thr ranks on the ice-binding face (Fig. 2). If the DPF difference between *Tm*AFP and ubiquitin (6.3–3.8) at 20 °C is ascribed to these 6 water molecules, they need to have a correlation (or residence) time of ~300 ps. This estimate is consistent with the assignment of the $^{17}O$ dispersions (at 27–50 °C) to internal water molecules, implying that the contribution from the 6 surface waters is frequency-independent up to 81 MHz. At temperatures approaching −30 °C, these water molecules would have correlation times of order 10 ns and would then not contribute to $R_1$ at 81 MHz, hence the convergence of the DPF profiles at low temperatures (Fig. 5).

Apart from the rank of 6 water molecules on the ice-binding face, the hydration of *Tm*AFP is unremarkable and does not differ significantly from the similarly sized protein ubiquitin. There is thus no evidence in our data that the hydration layer is more extended or more strongly perturbed for *Tm*AFP than for other proteins. If, for example, the observed relaxation enhancement were attributed to two water layers on the *Tm*AFP surface (with 50% more waters in the second layer for geometric reasons), we would obtain (with $N_H = 915$) a maximum DPF of 3.3 (rather than 9.6), leaving little room for the effect of the 6 strongly perturbed water molecules. We therefore conclude that the second layer is much less perturbed than the first layer.

Because the 6 water molecules are located in the middle of the ice-binding surface, they must have a direct effect on the antifreeze activity of *Tm*AFP. A computational study focusing on these water molecules did not record any exchange event during the rather short 400 ps MD trajectory of the fully solvated protein.[31] Since the simulation was performed at 0 °C, this result is not inconsistent with our conclusions (~300 ps residence time at 20 °C), especially if the uncertainty introduced by imperfect force fields is borne in mind. Interestingly, the simulation showed that the 6 water molecules are absent in the *Tm*AFP–ice complex, apparently because a better match to the ice surface is produced by the two Thr ranks when the intervening trough is empty. The main contribution of these water molecules to *Tm*AFP ice binding may therefore be entropic. Because the 6 water molecules are ordered both in position (their mean *B*-factor is almost as low as for the 5 internal waters: 17 *vs.* 15 Å$^2$)[26] and in orientation (due to strong H-bonds to adjacent Thr hydroxyls) their release would entropically favor binding. Furthermore, their H-bonds may reduce the configurational entropy of the Thr side-chains in the unbound state, again favoring ice binding.

While a high degree of order of the 6 water molecules makes binding stronger, a short residence time can make the binding faster. If the water molecules were much more long-lived, their release would become rate-limiting for binding of *Tm*AFP to the ice surface. The sub-nanosecond residence time of these water molecules inferred from our data may be essential for ensuring a high adsorption rate, which in turn may govern the non-equilibrium 'freezing point' (the temperature at which uncontrolled ice growth occurs).[9,10] In the computational study, it was proposed that the 6 water molecules move with the *Tm*AFP molecule as it approaches the ice surface and that they contribute to recognition and binding in the early stages of the encounter.[31] However, our experimental results indicate that the residence time of these water molecules is an order of magnitude shorter than the rotational correlation time of *Tm*AFP so they could hardly be said to move with the protein. Nevertheless, since the width of the ice–water interface corresponds to about 3 water layers,[16] the recognition and adsorption processes may be rather complex.

Even if the rank of 6 surface waters were to play a role in enhancing the antifreeze activity of *Tm*AFP, it is clearly not an indispensable feature. The ice-binding face of the non-homologous but structurally similar *Cf*AFP also features two Thr ranks (5 + 4 rather than 7 + 4) with the same 4.8 Å spacing along the helix axis, but the groove between the Thr ranks is more narrow than in *Tm*AFP (the Thr $O^{\gamma}$–$C^{\gamma}$ spacing is 3.9 *versus* 4.9 Å) and devoid of water.[47] In a recent MD simulation study, the hydration properties of *Cf*AFP were examined at +27 and −23 °C (in the absence of ice).[35] At both temperatures, the translational and rotational mobility of water molecules in the second hydration shell at the non-ice-binding surfaces were essentially the same as in bulk water. For the ice-binding surface, this was also true at +27 °C, whereas at −23 °C a significant perturbation was seen also in the second shell. For the ice-binding surface at −23 °C, the translational DPF was 2.4 in the first shell, 1.6 in the second shell and 1.1 in the third shell.

However, the outer boundaries of the first two shells were taken as 3.1 and 5.4 Å. These values are close to the first minima (outside the first peak) in the $O_W$–O and $O_W$–C pair distribution functions, respectively.[41] Considering that the ice-binding surface of *Cf*AFP contains 9 Thr methyls and an Ile side-chain, the first layer of water molecules contribute to both the first and second hydration shells as defined by these authors.[35] Therefore, the average translational DPF should be ~2 for the first hydration layer at the ice-binding surface and less for the other surfaces. This value is smaller than the rotational DPF deduced here at −23 °C (Fig. 5) for *Tm*AFP (~9) and even for ubiquitin (~4). The difference with respect to *Tm*AFP can be partly explained by the rank of 6 water molecules on the ice-binding surface of *Tm*AFP, which are not present in *Cf*AFP. The difference in DPF values between *Cf*AFP and ubiquitin can be explained by dynamic heterogeneity and the fact that the DPF averages the translational diffusion coefficient but the inverse of the rotational diffusion coefficient. Thus, the translational and rotational DPFs are biased by the fastest and slowest waters, respectively.[48] In summary, we propose that the simulation results for *Cf*AFP are consistent with our NMR results for *Tm*AFP: neither indicate significant perturbations beyond the first water layer and both reveal larger perturbations on the ice-binding face, with the most dramatic effects for *Tm*AFP due to the rank of 6 water molecules trapped between the two ranks of Thr residues.

## 5. Conclusions

The water $^{17}O$ spin relaxation data presented here provide the first experimental characterization of the hydration dynamics

 

of an antifreeze protein. For the hyperactive *Tm*AFP we find no evidence for unusual global hydration behavior, such as a particularly long-ranged perturbation or an ice-like hydration structure with accompanying slow dynamics. Our data do not necessarily exclude the possibility of specific structural features, such as an enhanced tetrahedral order in the hydration layer on the ice-binding face, as inferred from MD simulations of *Tm*AFP[35] and other AFPs,[49,50] as long as these structural modifications are not clearly manifested in the dynamics. However, we note that the increased tetrahedral order induced in bulk water on lowering the temperature into the supercooled regime is accompanied by a dramatic slowing down of the rotational motion.

While its global hydration behavior appears to be unremarkable, the crystal structure of *Tm*AFP reveals two unique hydration structures, both of which are characterized dynamically here. We find that 2 of the 5 rigidly enclosed internal water molecules exchange with a residence time of $8 \pm 1$ μs at 300 K and a large activation energy of $\sim 50$ kJ mol$^{-1}$, reflecting intermittent large-scale conformational fluctuations in the protein. The rank of 6 water molecules occupying the central trough on the ice-binding surface exchange with bulk water on a sub-nanosecond time scale. The combination of high order and fast exchange may allow these water molecules to contribute entropically to the ice-binding affinity without compromising the high absorption rate that is crucial for antifreeze activity.

## Acknowledgements

This work was supported by the Swedish Research Council, the Knut & Alice Wallenberg Foundation, and the Canadian Institutes for Health Research. P. L. D. holds a Canada Research Chair in Protein Engineering.

## References

1 Y. Yeh and R. E. Feeney, *Chem. Rev.*, 1996, **96**, 601–617.
2 J. G. Duman, *Annu. Rev. Physiol.*, 2001, **63**, 327–357.
3 P. L. Davies, J. Baardsnes, M. J. Kuiper and V. K. Walker, *Philos. Trans. R. Soc. London, Ser. B*, 2002, **357**, 927–935.
4 S. P. Graether and B. D. Sykes, *Eur. J. Biochem.*, 2004, **271**, 3285–3296.
5 D. Doucet, V. K. Walker and W. Qin, *Cell. Mol. Life Sci.*, 2009, **66**, 1404–1418.
6 J. A. Raymond and A. L. DeVries, *Proc. Natl. Acad. Sci. U. S. A.*, 1977, **74**, 2589–2593.
7 C. A. Knight and A. Wierzbicki, *Cryst. Growth Des.*, 2001, **1**, 439–446.
8 A. J. Scotter, C. B. Marshall, L. A. Graham, J. A. Gilbert, C. P. Garnham and P. L. Davies, *Cryobiology*, 2006, **53**, 229–239.
9 H. Nada and Y. Furukawa, *J. Phys. Chem. B*, 2008, **112**, 7111–7119.
10 C. A. Knight and A. L. DeVries, *Phys. Chem. Chem. Phys.*, 2009, **11**, 5749–5761.
11 M. Takamichi, Y. Nishimiya, A. Miura and S. Tsuda, *FEBS J.*, 2007, **274**, 6469–6476.
12 W. Blokzijl and J. B. F. N. Engberts, *Angew. Chem., Int. Ed. Engl.*, 1993, **32**, 1545–1579.
13 Y.-K. Cheng and P. J. Rossky, *Nature*, 1998, **392**, 696–699.
14 N. T. Southall, K. A. Dill and A. D. J. Haymet, *J. Phys. Chem. B*, 2002, **106**, 521–533.
15 D. Chandler, *Nature*, 2005, **437**, 640–647.
16 J. A. Hayward and A. D. J. Haymet, *Phys. Chem. Chem. Phys.*, 2002, **4**, 3712–3719.
17 B. Halle, in *Hydration Processes in Biology.*, ed. M.-C. Bellisent-Funel, IOS Press, Dordrecht, The Netherlands, 1998, pp. 233–249.
18 B. Halle, *Philos. Trans. R. Soc. London, Ser. B*, 2004, **359**, 1207–1224.
19 K. Modig, E. Liepinsh, G. Otting and B. Halle, *J. Am. Chem. Soc.*, 2004, **126**, 102–114.
20 C. Mattea, J. Qvist and B. Halle, *Biophys. J.*, 2008, **95**, 2951–2963.
21 M. Davidovic, C. Mattea, J. Qvist and B. Halle, *J. Am. Chem. Soc.*, 2009, **131**, 1025–1036.
22 B. Halle, V. P. Denisov and K. Venu, in *Biological Magnetic Resonance.*, ed. N. R. Krishna and L. J. Berliner, Kluwer Academic/Plenum, New York, 1999, vol. 17, pp. 419–484.
23 B. Halle, V. P. Denisov, K. Modig and M. Davidovic, in *Protein Folding Handbook*, ed. J. Buchner and T. Kiefhaber, 2005, vol. I, pp. 201–246.
24 D. H. Rasmussen and A. P. MacKenzie, in *Water Structure at the Water–Polymer Interface.*, ed. H. H. G. Jellinek, Plenum, New York, 1972, pp. 126–145.
25 Y.-C. Liou, P. Thibault, V. K. Walker, P. L. Davies and L. A. Graham, *Biochemistry*, 1999, **38**, 11415–11424.
26 Y.-C. Liou, A. Tocilj, P. L. Davies and Z. Jia, *Nature*, 2000, **406**, 322–324.
27 M. E. Daley, L. Spyracopoulos, Z. Jia, P. L. Davies and B. D. Sykes, *Biochemistry*, 2002, **41**, 5515–5525.
28 C. B. Marshall, M. E. Daley, L. A. Graham, B. D. Sykes and P. L. Davies, *FEBS Lett.*, 2002, **529**, 261–267.
29 M. Bar, Y. Celik, D. Fass and I. Braslavsky, *Cryst. Growth Des.*, 2008, **8**, 2954–2963.
30 E. Persson and B. Halle, *J. Am. Chem. Soc.*, 2008, **130**, 1774–1787.
31 Z. Yang, Y. Zhou, K. Liu, Y. Cheng, R. Liu, G. Chen and Z. Jia, *Biophys. J.*, 2003, **85**, 2599–2605.
32 B. Jacobson, *Nature*, 1953, **172**, 666–667.
33 I. M. Klotz, *Science*, 1958, **128**, 815–822.
34 E. H. Grant, *Ann. N. Y. Acad. Sci.*, 1965, **125**, 418–427.
35 D. R. Nutt and J. C. Smith, *J. Am. Chem. Soc.*, 2008, **130**, 13066–13073.
36 Y.-C. Liou, M. E. Daley, L. A. Graham, C. M. Kay, V. K. Walker, B. D. Sykes and P. L. Davies, *Protein Expression Purif.*, 2000, **19**, 148–157.
37 D. E. Woessner, *J. Magn. Reson.*, 1980, **39**, 297–308.
38 G. Carlström and B. Halle, *Langmuir*, 1988, **4**, 1346–1352.
39 R. Abseher, H. Schreiber and O. Steinhauser, *Proteins: Struct., Funct., Genet.*, 1996, **25**, 366–378.
40 C. Schröder, T. Rudas, S. Boresch and O. Steinhauser, *J. Chem. Phys.*, 2006, **124**, 234907.
41 J. Qvist and B. Halle, *J. Am. Chem. Soc.*, 2008, **130**, 10345–10353.
42 J. Garcia de la Torre, M. L. Huertas and B. Carrasco, *Biophys. J.*, 2000, **78**, 719–730.
43 B. Halle and M. Davidovic, *Proc. Natl. Acad. Sci. U. S. A.*, 2003, **100**, 12135–12140.
44 V. P. Denisov and B. Halle, *Faraday Discuss.*, 1996, **103**, 227–244.
45 V. P. Denisov, J. Peters, H. D. Hörlein and B. Halle, *Nat. Struct. Biol.*, 1996, **3**, 505–509.
46 V. P. Denisov, K. Venu, J. Peters, H. D. Hörlein and B. Halle, *J. Phys. Chem. B*, 1997, **101**, 9380–9389.
47 E. K. Leinala, P. L. Davies and Z. Jia, *Structure*, 2002, **10**, 619–627.
48 E. Persson and B. Halle, *Proc. Natl. Acad. Sci. U. S. A.*, 2008, **105**, 6266–6271.
49 C. Yang and K. A. Sharp, *Biophys. Chem.*, 2004, **109**, 137–148.
50 N. Smolin and V. Daggett, *J. Phys. Chem. B*, 2008, **112**, 6193–6202.

Supplementary Material (ESI) for PCCP


# High water mobility on the ice-binding surface of a hyperactive antifreeze protein

## Supplementary Information: Further experimental details

Kristofer Modig, Johan Qvist, Christopher B. Marshall, Peter L. Davies and Bertil Halle

**Table S1.** Amino acid composition of *Tm*AFP samples A and B. [a]

| Amino acid | Sequence | Sample A | Sample B |
|---|---|---|---|
| Ala | 9 | 9.0 | 9.2 |
| Arg | 0 | 0.1 | 0.1 |
| Asx | 11 | 11.5 | 11.4 |
| Gly | 7 | 8.1 | 8.1 |
| Glx | 4 | 6.1 | 6.4 |
| His | 2 | 2.0 | 2.1 |
| Ile | 0 | 0.4 | 0.4 |
| Leu | 0 | 0.3 | 0.2 |
| Lys | 3 | 3.1 | 3.1 |
| Met | 0 | 0.7 | 0.8 |
| Phe | 1 | 1.0 | 1.0 |
| Pro | 2 | 2.5 | 3.3 |
| Ser | 6 | 6.6 | 6.5 |
| Thr | 19 | 18.7 | 18.6 |
| Tyr | 1 | 0.9 | 1.0 |
| Val | 3 | 3.4 | 3.3 |

[a] Sample B was analyzed 6 years after sample A.

**Table S2.** Water $^2$H relaxation rate from *Tm*AFP samples A and B.[a]

| | Relaxation rate, $R_1$ ($s^{-1}$) | | |
|---|---|---|---|
| $\nu_0$ (MHz) | Sample A | Sample B uncorrected | Sample B corrected [b] |
| 4.58 | 2.84 | 2.76 | 2.83 |
| 6.86 | 2.80 | 2.71 | 2.77 |
| 11.96 | 2.68 | 2.62 | 2.68 |

[a] Sample B was measured 6 years after sample A.

[b] Corrected for lower solvent deuterium fraction by multiplication with viscosity ratio $\eta(X_D=0.476) / \eta(X_D=0.369) = 1.022$ (at 27 °C).

**Table S3.** Water $^{17}$O relaxation rate at 81 MHz before and after emulsification.

| | Relaxation rate, $R_1$ ($s^{-1}$) [a] | |
|---|---|---|
| Sample | Before | After |
| Reference | 1499 | 1502 |
| Sample B | 1569 | 1572 |

[a] Estimated experimental uncertainty ± 5 $s^{-1}$.

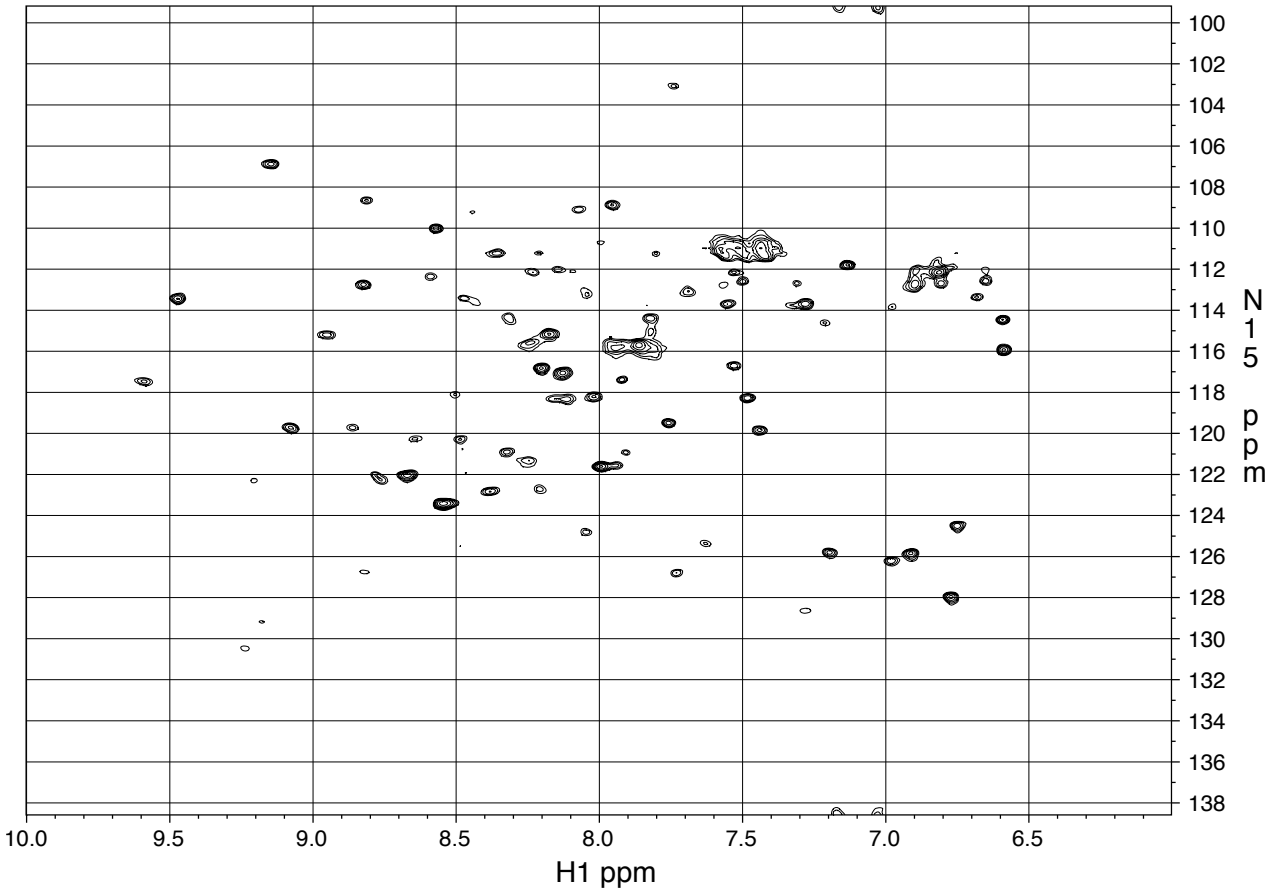


**Figure S1.** $^{1}H$–$^{15}N$ heteronuclear multiple-quantum coherence (HMQC) correlation spectrum of *Tm*AFP sample B (at natural $^{15}N$ abundance) recorded at 600 MHz after the MRD experiments.